Aeroelastic Investigation of a Utility Aircraft

Giuseppe Borrelli

Royal Institute of Technology, 100 44 Stockholm, Sweden
Email: borrelli@kth.se

Abstract

The following report aims to present the results obtained after a Structural-Aeroelastic analysis of the Twin Otter DHC-6, presenting also alternative designs which can lead to better development.
Starting from a given FEM model it was possible to extend it in order to design a new structure. Equations of Motion for a flexible body were employed to derive important relations to proceed with the investigation.
First, these allowed to demonstrate that the chosen design is not affected by aeroelastic instabilities, i.e. that divergence and reversal speeds are acceptable, whilst flutter is not encountered. Furthermore, it was proved that the wing can withstand significant loads all over the flight envelope.
Improvements were achieved by implementing a tapered spar design and a reduced wing box thickness, making it possible to significantly increase the maximum payload allowed. Still, a similar investigation to the previous one was carried out, validating the new structure and pointing out stresses as the main limiting factor.

1 Introduction

The design process of an aircraft includes interactions between several features, such as aerodynamics, flight dynamics, structures, controls and so on.

One assumption to deal with a simpler model is to consider a rigid body which moves in the fluid. This idealisation hardly applies to reality; indeed, the great majority of structures for aerospace applications often presents a light-weight design.
Due to this, deformations of the structure lead to a change in shape that, consequently, disturb the flow in the surrounding of the aircraft, changing the aerodynamic forces.

Aeroelasticity deals with the *reciprocal interaction* between a flexible structure and the unsteady flow with which it interacts. Having a flexible structure might not be a problem in most cases but it may lead to stability issues in some others and, eventually, result in failure. These issues may be classified as *static* or *dynamic*.

Static Aeroelasticity: The balance between fluid loads acting on the deformed shape and the internal elastic forces can lead to a convergence of these two responses.
Stability issues arise when the deformation taken into account leads to an increase of the aerodynamic loading, with a consequent increase of deformations. Problems of this type are *divergence* and *aileron reversal*.

- *Divergence*: At high speed, by loading the wing structure, the elastic deformation leads to an overall increase of the incidence, which changes the load distribution, so that the wing experience an even higher deformation (highest at the tip). It's straightforward to understand how this self-amplifying mechanism will lead to the failure.
  To avoid this effect, it is important to never exceed the *divergence speed*. This limit can be raised by either increasing the structural stiffness or by modifying the wing shape (e.g. backward swept wing).

- *Aileron Reversal*: This phenomenon is related to the reduction of ailerons' efficiency with increasing flight speed.
  As a consequence of a downwards deflection of a trailing edge control surface, together with an increase in lift, also a pitch down torque is introduced (indeed, a direct consequence of the structure's *flexibility*), which reduces the local angle of attack, counteracting the desired input.
  Once that the *reversal (critical) speed* is exceeded, the effect of the deflection will be the opposite than the desired one.

Dynamic aeroelasticity: On the other hand, an aeroelastic system can oscillate when combining structural vibrations with unsteady aerodynamic loads generated by this same motion. The system may still be

statically stable but dynamically unstable, since the amplitude of the oscillations might grow in time.
This phenomenon is known as *flutter*.
Given the complex physics of unsteady flow, different *flutter* instabilities are encountered:

- *classical flutter*: dealing with a vibrating lifting surface extracting energy from the surrounding flow, having an exponential growth of oscillations.

- *stall flutter*: related to dynamic flow separation.

- *transonic flutter*: related to interactions of moving shocks and boundary layer separations. *Transonic dip* occurs at Mach close to 1.

- *buffeting*: due to highly turbulent unsteady flow creating strong disturbances upstream of a lifting surface.

The last three phenomena are also described as *non-linear* flutter, since they depend on steady flow condition and initial deformation. Coupling effects between instabilities can also occur.

2 The Aeroelastic Model

In order to perform an aeroelastic analysis it is necessary to define some steps with the purpose to obtain good predictions of what will happen to the real structure.

A *discrete aeroelastic model* needs to be implemented, by means of which it will be possible to test different design configurations and see how they affect the overall aeroelastic behaviour.
The given model contains information about the degrees of freedom, the structural and aerodynamic matrices, the material properties, the geometry and so on. Once this elements are defined, it is possible to derive relationships from the equations of motion (*EOMs*) and to employ them to accomplish the aeroelastic investigation.

2.1 Equations of Motion

The model utilizes a *finite element discretization* approach to express a set of elastic degrees of freedom (*dofs*), namely: $w(y,t)$, deflection, $\varphi(y,t)$, bending slope, and $\theta(y,t)$, twist.
As a discretization method, the *strip theory* is employed. This theory utilizes a *two-dimensional* analysis together with a *beam model* and it is able to evaluate critical speeds, with the benefit of providing (usually) conservative results.

Inertial, elastic and aerodynamic forces are acting on the considered structure. Given the equilibrium condition, they read as:

$$\boldsymbol{f}_i(\boldsymbol{v},\dot{\boldsymbol{v}},\ddot{\boldsymbol{v}}) + \boldsymbol{f}_e(\boldsymbol{v}) + \boldsymbol{f}_a(t,\boldsymbol{v},\dot{\boldsymbol{v}}...) = 0 \tag{1}$$

Matrix representation is available when expressing the increments of elastic restoring forces ($\Delta\boldsymbol{f}_e$) given a deformation ($\Delta\boldsymbol{v}$) and of inertial forces ($\Delta\boldsymbol{f}_i$) given a structural acceleration ($\Delta\ddot{\boldsymbol{v}}$):

$$\Delta\boldsymbol{f}_e = -\boldsymbol{K}\Delta\boldsymbol{v} \qquad \Delta\boldsymbol{f}_i = -\boldsymbol{M}\Delta\ddot{\boldsymbol{v}}$$

where $\boldsymbol{K}$ and $\boldsymbol{M}$ represent the stiffness and the mass matrices, respectively.
Generally, the same matrix representation, based on the linear assumption, is not possible when looking at time-domain unsteady aerodynamic forces.
With these considerations in mind, the equilibrium condition in (1) is now revised as:

$$\boldsymbol{M}\ddot{\boldsymbol{v}} + \boldsymbol{K}\boldsymbol{v} = \boldsymbol{f}_a(t,\boldsymbol{v},\dot{\boldsymbol{v}}...) \tag{2}$$

Shifting to the **frequency domain**, by taking the *Laplace transform*[1] of the time-domain *EOMs*, the analysis gets more significant. Equation (2) becomes:

$$\boldsymbol{M}p^2\hat{\boldsymbol{v}} + \boldsymbol{K}\hat{\boldsymbol{v}} = q\boldsymbol{Q}(p)\hat{\boldsymbol{v}} \tag{3}$$

with $\boldsymbol{Q}(p)$ as the aerodynamic matrix, q the dynamic pressure, $\hat{\boldsymbol{v}}$ the mode-shape and $p = \sigma + i\omega$ as the Laplace variable (σ as damping, ω as angular frequency).

Physical remarks can be carried out once a *complex-valued Ansatz* is formulated, that is to say:

$$\boldsymbol{v}(t) = \hat{\boldsymbol{v}}e^{pt} \quad \text{with} \quad e^{pt} = e^{\sigma t}(\cos\omega t + i\sin\omega t) \tag{4}$$

It's straightforward to assess a stability criterion which states that the motion is: damped when $\sigma < 0$; at constant amplitude for $\sigma = 0$ and growing in time if $\sigma > 0$.

2.2 Vibration testing

The reliability of the employed model needs to be supported by structural testing. Characteristic frequencies of the structure are verified experimentally and compared to the ones obtained from the solution of the *vibration eigenvalue problem* in (5). This procedure is carried out by exciting the structure and measuring the response with accelerometers placed in strategic positions (e.g. bending on mid-line, torsion at leading edge).

Excluding damping ($\sigma = 0$) and aerodynamic loads, the information contained in (3) reduce to:

$$[\boldsymbol{K} - \omega^2\boldsymbol{M}]\hat{\boldsymbol{v}} = 0 \tag{5}$$

[1] Where the Laplace transform of a time-signal is performed as: $x(p) = \int_0^\infty e^{-pt}x(t)dt$

with the displacement in the time domain which reads as: $\boldsymbol{v}(t) = \hat{\boldsymbol{v}}e^{i\omega t}$.

This procedure allows to *"tune"* the material properties of the model, such as E and G, so to have a more accurate analysis. It shows also the relevance of mutual juxtaposition between experiments and modelling.

2.3 Static Aeroelasticity

It is now possible to exploit what derived in previous sections and to develop it for the aeroelastic investigation.

Static Aeroelasticity deals with steady state conditions, i.e. $\ddot{\boldsymbol{v}} = 0$. It is important to notice how the inertial forces, thus $\boldsymbol{M}$, do not play a role at this point. Expression (2) is simplified to:

$$\boldsymbol{K}\boldsymbol{v} = \boldsymbol{f}_e \tag{6}$$

Where $\boldsymbol{f}_e$ corresponds to the external applied forces.
Contributions to $\boldsymbol{f}_e$ are given by aerodynamic forces due to elastic deflection $\boldsymbol{v}$ and control surface deflection δ: $\boldsymbol{f}_a = q\boldsymbol{Q}_0\boldsymbol{v} + q\boldsymbol{f}_0\delta$; aerodynamic forces due to small changes of the reference geometry $\boldsymbol{f}_{a0}$ (e.g change in angle of attack) and weight distribution $\boldsymbol{f}_w$.

An important parameter to be defined is the reduced frequency:

$$k = \frac{\omega c}{2u} = \frac{\omega b}{u} \tag{7}$$

This non-dimensional quantity accounts for how fast the wing is oscillating with respect to the speed of flight. In steady state ω is equal to zero, thus $k = 0$.

Aeroelastic divergence: as already explained in the introduction, once the divergence speed of flight is reached, forces due to elastic displacement will overcome the restoring ones.
Mathematically, this can be studied by considering equation (3) in the case where no damping is present and $k = 0$ (thus, when the oscillatory motion of the body is not taken into account). Furthermore, for the *static* analysis, the aerodynamic matrix does not depend on the *heave* motion, so that $\boldsymbol{Q}(k)$ is represented by $\boldsymbol{Q}_0$.
The *EOM* in (6) is now:

$$[\boldsymbol{K} - q\boldsymbol{Q}_0]\boldsymbol{v} = 0 \tag{8}$$

The smallest *real* eigenvalue, for which the matrix become singular, is q_D (*divergence dynamic pressure*) to which correspond the eigenvector $\boldsymbol{v}_D$. If $q > q_D$, the solution will be unstable, leading to an infinite displacement $\boldsymbol{v}$.

Computationally speaking, having $\boldsymbol{Q}_0$ typically as a singular matrix, it is better to solve:

$$[\boldsymbol{Q}_0 - \frac{1}{q}\boldsymbol{K}]\boldsymbol{v} = [\boldsymbol{Q}_0 - \lambda\boldsymbol{K}]\boldsymbol{v} = 0$$

where q_D is computed as inverse of the largest real λ.

Aileron Reversal: downwards deflection of the flap to produce rolling moment results in an elastic twist which introduces a *pitch-down* effect (vice versa on the opposite wing, for which the flap deflects upwards). Once the *aileron reversal speed* is encountered, the rolling moment is the opposite with respect to the intended one.
The aerodynamic forces coming into play are related to the deflection of the ailerons δ so that the eigenvalue problem is:

$$[\boldsymbol{K} - q\boldsymbol{Q}_0]\boldsymbol{v} = q\boldsymbol{Q}_0\delta \tag{9}$$

By knowing that the rolling moment coefficient (C_R) is given by the contribution of the elastic deformation and of the deflection of the control surface:

$$C_R = \boldsymbol{C}_{Rv}^T\boldsymbol{v} + C_{R\delta}^T\delta$$

and noticing that $C_R = 0$ is a condition for reversal, the deflection can be expressed as a function of $\boldsymbol{v}$:

$$\delta(R = 0) = -\frac{\boldsymbol{C}_{Rv}^T}{C_{R\delta}^T} \cdot \boldsymbol{v} \tag{10}$$

And plugging (10) into (9), defining $\boldsymbol{Q}_\delta = -\boldsymbol{f}_0\boldsymbol{C}_{Rv}^T/C_{R\delta}^T$, the problem to be implemented is:

$$[\boldsymbol{K} - q(\boldsymbol{Q}_0 + \boldsymbol{Q}_\delta)]\boldsymbol{v} = 0 \tag{11}$$

It is really important, at this stage of the analysis, to have accurate material properties so to allow for meaningful predictions.

2.4 Flutter Analysis

Eventually the flutter phenomenon can be studied. For this last case it is necessary to introduce unsteady aerodynamics. The description accounts for the time-domain characterization of the aerodynamic forces $f_a(t)$. However, frequency-domain analysis is more significant when dealing with stability. This will lead to the following *non-linear* eigenvalue problem:

$$\boldsymbol{F}(p)\hat{\boldsymbol{v}} = [\boldsymbol{M}p^2 + \boldsymbol{K} - q\boldsymbol{Q}(\hat{p})]\hat{\boldsymbol{v}} = 0 \tag{12}$$

where p is the eigenvalue making the flutter matrix $\boldsymbol{F}(p)$ singular. The reduced Laplace variable $\hat{p} = pb/u$ is introduced and it defines a parameter in the description of the aerodynamic matrix $\boldsymbol{Q}(\hat{p})$.
From the flutter equation, it is easily verifiable how the case of $q = 0$ leads back to the *vibration eigenvalue problem* in (5).

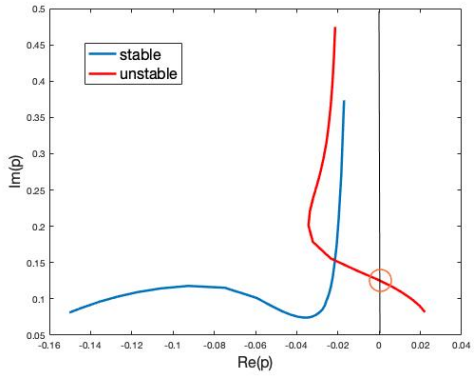

Figure 1: Root locus with Stable and Unstable evolution of flutter modes.

When plotting the evolution of p on an imaginary plane it is possible to observe how, by increasing the airspeed, the eigenvalues can either move further on the left, i.e. become more stable, or cross the imaginary axis, generating a *flutter instability*. Once the crossing occurs, the eigenvalue will have real part equal to zero, i.e. $p = \omega_F$, with ω_F as the *angular flutter frequency*. This behaviour is illustrated in figure 1

The big difference compared to previous cases is that flutter analysis aims at *tracking the complex eigenvalues*, meaning that the interaction with aerodynamic forces brings to a *phase shift* between different *dofs*.

From the numerical aspect, several methods are available. One example is the *Doublet-Lattice method (DLM)* which employs an unsteady potential flow model accounting also for 3D effects.
Beside this, an approximated eigenvalue problem can be solved for $\hat{p}$ (non-dimensional) utilizing the *strip theory model*. With the assumption of having $\boldsymbol{Q}(k)$ available for the different reduced frequencies, problem (12) becomes:

$$\left[\left(\frac{u}{b}\right)^2 \boldsymbol{M}\hat{p}^2 + \boldsymbol{K} - q\boldsymbol{Q}(k)\right]\hat{\boldsymbol{v}} = 0 \tag{13}$$

The so-called **p-k method** is developed for the iterative solution to obtain k. For a given q and fixed (assumed) k, after defining the upper and lower bounds of k_j, it solves the approximated eigenvalue problem in (13) for $\hat{p}_j^2$. The solutions $\hat{p}_j$ with positive frequency are considered (indeed, only $\omega > 0$ has a physical meaning) and are used to check if:

$$Im\{\hat{p}_j(k)\} = k \tag{14}$$

If this is not the case, the procedure has to be carried out again with another k.
Once equation (14) is verified, the problem is evaluated again for other air speeds.

The procedure depicted is very expensive in case of real aircraft structures, where the number of elements (and, consequently, *dofs*) is very high (99 elements have been used for the project, to have a convergence of the solution).
A *Modal Flutter analysis* can be an alternative. First the solution of problem (5) is found (much easier to solve because matrices are not sparse). Being aeroelastic motion dominated by low-frequency modes, it is possible to set a chosen number of modal coordinates in order to reduce the size of the flutter eigenvalue problem (*projecting* accordingly matrices $\boldsymbol{M}$ and $\boldsymbol{K}$). Other improvements are obtained by applying alternative methods (e.g bisection or Newton's method) to solve the non-linear problem in (14).

We have now developed a useful toolbox, underlying all the relevant information and the necessary steps which are required in order to compute an *Aeroelastic Analysis*.
In the following sections, these tools will be used in order to perform the design of a 19-seats utility aircraft.

3 Design of the Aircraft

The example employed for the analysis is the De Havilland Canada DHC-6 Twin Otter, shown if Figure 2.
Main goal is to select reasonable dimensions of the structure in such a way that the aircraft is stable from the aeroelastic point of view. Furthermore, the aircraft has to withstand relevant loads which might be encountered during the flight envelope.

Figure 2: De Havilland Canada DHC-6 Twin Otter.

Some other limits are reported in Table 1, such as the the take-off weight and the maximum velocity allowed.

Maximum take-off weight	5670 kg
Cruise speed	150 knots
Maximum speed (v_{ne})	200 knots

Table 1: Specifications for Utility Aircrafts (CS-23).

3.1 Structural design

The first component to be modelled is the *main wing* of the aircraft. Here, it is important to have a good structure, which is able to support the loads due to either *torsion* and *bending*.
Some assumptions may be done concerning the wing box. First of all, the chord ($c = 1.9697$ m) remains constant all along the span ($l = 19.8$ m), leading to a rectangular planimetry ($S = 39$ m^2). The wing box itself can be divided into two contributions: the *skin sheets* and the *spar*, as shown in figure 3.

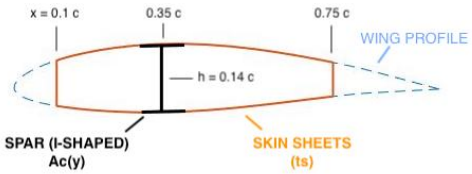

Figure 3: Wing box: simplified structure.

Torsion loads are carried exclusively by the wing skin sheets. The thickness of the sheets (t_s) is usually considered as constant along the whole span (this also helps with a simpler manufacturing), so that the stiffness term GK remains constant throughout the whole wing.
Both the skin and the wing spar, instead, help in the withstanding of the bending loads. The spar is here simplified as a *thin-web I-beam*, with $A_c(y)$ as the total cross section area of the two spar caps.

The material which is employed for the wing is the aluminum alloy 2024-T3, whose favorable fatigue properties are beneficial for components subjected to repeated loads. The main properties of this material are summarized in Table 2.

Density (ρ)	2780 kg/m^3
Young's modulus (E)	73.1 GPa
Shear modulus (G)	26 GPa
Ultimate Tensile Strength	483 MPa
Shear Strength	283 MPa

Table 2: Al 2024-T3 properties.

Beyond the main wing, when modelling the total mass and total inertia of the aircraft, contributions from the *engine nacelles* (1), the *fuel* (2), the *minimum payload* - 100 kg (3), the *fuselage* (4) and the *horizontal tail plane* - HTP (5) are taken into account. This data is shown in the following table [2] (the values are approximated to the second digit):

	m [kg]	x [m]	y [m]	J_x [kgm^2]	J_y [kgm^2]
1	330 (x2)	-2.28	$\pm$ 2.85	250	650
2	1170	-1.08	0	292.5	3381.3
3	100	-1.08	0	25	289
4	1451.5	-2.62	0	362.87	4194.7
5	258.54	7.52	0	64.64	747.18

Table 3: Concentrated masses.

Table 3 collects the values for the mass, the x and the y position with respect to the mid-chord (of the main wing) and the Roll (J_x) and Pitch (J_y) inertia, for each one of the concentrated masses. The locations of these masses are then re-defined in the finite element code, with respect to the elastic axis (here located at 35% of the chord).

A final contribution to the overall mass is given by the *equipment* (fittings, control system parts, de-icing and electrical devices). The latter is modelled as a distributed mass: $m_e = 10$ kg/m; and the associated distributed inertia: $J_y = 3.5$ kgm.
Ailerons are considered only for the outer half of the semi-wing-span. They're hinged at 80% of the chord. The mass of the hinges has been neglected.

3.2 Sizing of the Structure

At this stage of the modelling we focus on the dimensions needed to describe the main wing. It is important that the sizing of the structure is such that it allows to have results which are acceptable from both the aeroelastic and the structural point of view.

As a first approach, the dimensions have all been chosen as constant values.
The *I-shaped* beam is characterized by the the sizes of the spar caps, which have an height and a base (*hspar* and *bspar* respectively - *see code*), the thickness (*tspar*) and the height (h) of the thin web in between (see Table 4).

A_c [m^2]	*hspar* [m]	*bspar* [m]	h [m]	*tspar* [m]
0.01	0.01	0.5	0.2758	0.005

Table 4: *I-beam* cross section.

[2] Here the contributions of the tail and of the fuselage has been divided with respect to the given data in the description.

In order to describe the stiffness of the wing, inertia's properties have been computed.
Formulas related to the *I-beam* are available. The latter contributes to the bending response.
The wing box, instead, has been approximated with an *hollowed ellipsoid*, for which formulas for inertia are tabulated. The dimensions of this element are the length of the major and minor axis, divided by two. In the code, they reads as $a\_ell = 0.6402$ m and $b\_ell = 0.1379$ m, respectively. The thickness of the skin is of $t_s = 0.001$ m and, together with the previous two values, characterize both the bending and torsional contribution of the wing box to the total stiffness.

3.3 Horizontal Tail Plane and Boundary Conditions

An accurate load analysis has to take into account suitable boundary conditions. In the case of a wing test performed in the lab, it is straightforward to assign boundary conditions so that the structure is clamped on one side.

More effort has to be done for a free flying aircraft. Boundary conditions, as described into the code, depict the rigid pitch and roll motion, together with the continuity of the slope of the deformations at the nodes.
Once the aerodynamic loads are introduced, the flexible structure will deform (even if not rigidly constrained), thanks to the interaction between inertial, elastic and aerodynamic forces. Mass and stiffness modelling plays a crucial role in this investigation.

Finally, before moving to the results, it is useful to point out how the tail (HTP) affects the overall aerodynamics. The flexibility of the HTP may be assumed to be much smaller with respect to the one of the main wing (due to smaller Aspect Ratio).
A single elements is considered, with two nodes and, consequently, 6 *dofs*. The aerodynamic of the element is retrieved utilizing the function *'beam_amatrix.m'* which requires as inputs the reduced frequency, the span and the local position of the elastic axis (zero for HTP). The reduced frequencies have to be scaled, with reference to the main wing, according to:

$$k_{tail} = k\frac{c_{tail}}{c} \tag{15}$$

where $c_{tail} = 1.48$ m represents the chord of the tail. The span is obtained knowing that the $S_T = 9.3$ m^2 is the area of the HTP.
Once the tail's aerodynamic matrix is know, it has to be introduced in the correct position in the general matrix - index *'r'* in *'Otterwing.m'* code.
The HTP modelling requires further considerations when attempting a *gust analysis*. For this scenario, the tail wing encounters the gust with a time delay, which has to be considered.

With these specifications, the total mass of the wing sums up to 992.042 kg, which, together with the concentrated masses in Table 3, allows for a total payload of 1037.96 kg. The torsional inertia is 121.641 kgm^2.
Aeroelastic constraints and certification limits are satisfied by this design. These analyses will be illustrated in the following section.

4 Aeroelastic and Loads Analyses

4.1 Divergence, Reversal and Flutter

In order for a structure to be certified, it is necessary to prove that it is free from flutter and it doesn't experience divergence and control reversal in the allowed range of speeds.

A first evaluation might come from a simulation performed on a *Finite Element Model*, as done for this project. Full scale tests will be required, consequently, for most of the cases, in order to verify the *FEM* predictions.

Before analysing the specific phenomena, it is wise to check the resulting frequencies derived from the *vibration eigenvalue problem*. These are reported in Table 5 for the first six modes (obtained as $f = \sqrt{\omega^2}/2\pi$), and are reasonable.

f [Hz]	1.187	2.233	3.617	6.26	11.617	18.479

Table 5: Structure's frequencies after vibration eigenvalue problem.

The Aeroelastic analysis has been carried out after having included the Horizontal Tail Plane in the modelling. By comparing the results with and without HTP, the values don't differ substantially.
This can be associated with the idea that that the majority of the lift is still produced by the main wing, which, then, will experience approximately the same deformation (different goes for the moment, as explained in section 4.2).

The velocities in Table 6, for *Divergence* and *Reversal*, are both acceptable, since they comply with the requirement of being larger than $1.15v_{ne}$.

u_{div}	230.89 m/s
u_{rev}	164.51 m/s

Table 6: Divergence and Reversal speeds.

More insights can be obtained on the Aileron Reversal by looking at the plots in Figure 4 and 5. Here it is clearly visible how, with the increase of the speed (and, then, of q_{dyn}) the efficiency of the rolling maneuver decreases, up to the point where it cancels out. In figure 5 the comparison with the *ideally* rigid wing is shown. Whilst for this case the rolling moment should increase indefinitely, in reality flexibility comes into play.

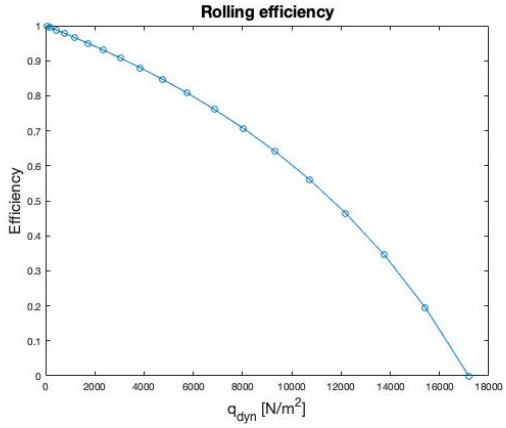

Figure 4: Aileron efficiency with increasing dynamic pressure.

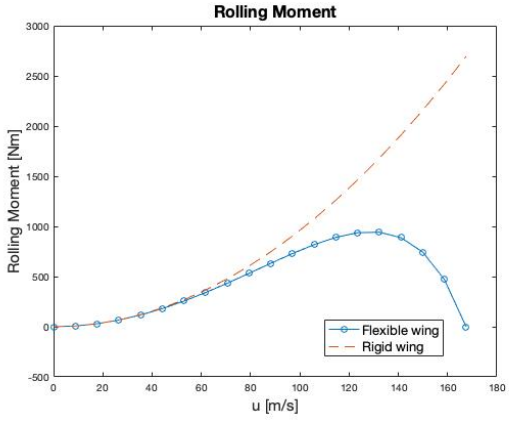

Figure 5: Rolling moment with increasing speed.

To continue, *Flutter* has been considered.
By performing a *Modal* analysis *up to the divergence speed* it is possible to conclude that the design of the Twin Otter's main wing is *not* affected by flutter. Indeed the crossing, as shown in figure 1, never occurs, because the real part of the eigenvalues remains negative as velocity increases. This behaviour is shown in figure 6 for the first four reduced frequencies.

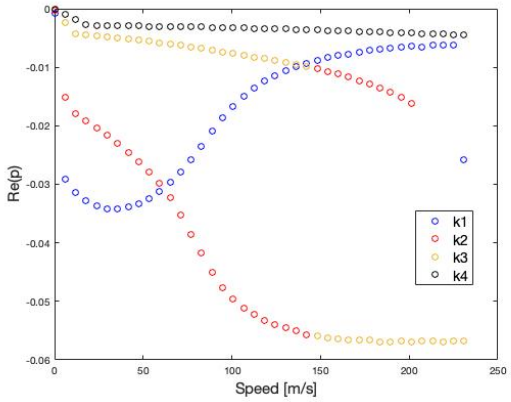

Figure 6: Evolution of the Real Part of the eigenvalues with velocity.

Being free from flutter, it is not needed to add concentrated masses in order to have aeroelastic stability. Thus, the total payload allowed remains unchanged.

4.2 Quasi-Steady Maneuvers

Now that the aircraft is stable from the aeroelastic point of view, we can continue the analysis by looking at the trim computation. This results into the rigid angle of attack (α) and the deflection of the elevator (δ_e), together with the displacement vector ($\boldsymbol{v}(y)$). The latter will be used to obtain the stress distribution and evaluate the *safety coefficient* for the most critical flight condition.

For this analysis, the modelling of the HTP has not been take into account. This choice is due to the fact that the values of lift and moment coefficients generated from the elevator deflection, have been assumed to be equal to $C_{l,\delta_e} = 0.608\ rad^{-1}$ and $C_{m,\delta_e} = -1.74\ rad^{-1}$ (see reference 3). The coefficients for the main wing have been calculated, instead, as $\boldsymbol{e_1}^T \boldsymbol{Q_o} \boldsymbol{e_3}/S$ and $\boldsymbol{e_3}^T \boldsymbol{Q_o} \boldsymbol{e_3}/S$ [3], resulting in $C_{l,\alpha} = 6.28\ rad^{-1}$ and $C_{m,\alpha} = -1.24\ rad^{-1}$ (respectively $5.66\ rad^{-1}$ and $-1.31\ rad^{-1}$, as tabulated values). If accounting for the $\boldsymbol{Q_o}$ with also the HTP effect, a big difference would have been noticed in the calculation of $C_{m,\alpha}$, which results to be equal to $-9.47\ rad^{-1}$, substantially different from the tabulated one. This can be linked to the fact that, even if the lift contribution from the tail is not significant, once this is multiplied by the distance to the main wing (nearly 8 m), the influence on moment becomes relevant.

The *Static Aeroelastic Trim* computation has been performed for different maneuver, namely: *cruise* ($n = 1$), *pull-up* ($n = 4.4$) and *descent* ($n = -1.6$).

[3] Vectors $\boldsymbol{e_1}$ and $\boldsymbol{e_3}$ selects only the elements of the matrix $\boldsymbol{Q_o}$ related to the deflection or to the twist, alternatively. The matrix $\boldsymbol{Q_o}$ is the aerodynamic matrix associated to the steady state - *See code.*

n	α [deg]	δ_e [deg]	C_{Ltrim}	v_{corner} [m/s]
1	3.11	-6.29	0.34	36.5
4.4	7.72	-15.60	0.85	76.5
-1.8	-3.16	6.38	0.35	49

Table 7: Trimmed conditions for different load factors. $v_{cruise} = 76.5$ m/s used for case 1. $v_{ne} = 102$ m/s for $n = 4.4$ and $n = -1.8$.

By recalling flight mechanics notions, the information stored in Table 7 are reasonable.
Consider the case of *steady pull-up* maneuver, for instance. The angle of attack has to be increased with respect to the *cruise* condition, so that more lift is generated and a climbing trajectory can be initiated. To support this, the elevator deflects upwards (negative δ_e), introducing a pitch-up moment.

In all three cases, the *aerodynamic limit*, i.e. $C_{Ltrim} < 1.5$, is observed. On the contrary, the last column of the table shows when this limit is not respected anymore. The *corner speed* is, indeed, the minimum velocity at which a given maneuver can be performed. When velocity is lower, the wing will experience *aerodynamic stall*.
Deflection of the elevator is always below the tabulated limit ($\delta_e = \pm 20$ deg) and saturation of the control is, thus, not reached.

Finally, the analysis includes also the effects of *inertial relief*. By doing so the stress evaluation accounts also for the distribution of the inertial loading (as the engine nacelles, in this case), that will help to reduce the stresses experienced by the main wing.

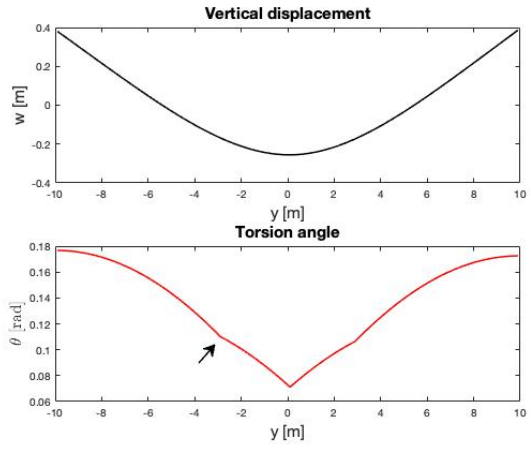

Figure 7: Plots for $w(y)$ and $\theta(y)$ for $n = 4.4$ and $u = 102$ m/s. *Inertial Relief* is highlighted.

This phenomenon is pointed out in figure 7 (more visible when considering the torsion angle). The beneficial effect is more evident when moving towards the wing root, where the stress level reaches critical values.

The last two graphs will be the starting point for the follow-up study, where the stresses will be computed and the most critical condition for the structure will be evaluated.

4.3 Stresses analysis

Once Aeroelastic and Aerodynamic limits have been verified, it is necessary to demonstrate that the structure can *safely* withstand the loads acting on it.

This procedure starts from the results obtained from the static trim performed in previous section (figure 7), where also the equations of motion have been utilized.
The output displacement vector ($\boldsymbol{v}(y)$) is C^1 continuous. This means that the second derivative will not ensure a continuous description (needed to compute normal stresses, for instance). Due to this, *shape functions* have to be introduced, both for bending ($\boldsymbol{N_w}(\xi)$) and torsion ($\boldsymbol{N_\theta}(\xi)$) deformations. These functions are expressed in terms of the local element coordinate ξ, given by: $\xi = (y - y_1)/l_e$, with l_e as the length of the element obtained after the discretization (so that $d\boldsymbol{N}(\xi)/dy = (d\boldsymbol{N}(\xi)/d\xi)/l_e$).
Having this description of displacements, bending moment ($M_b(t, y)$) and twist moment ($M_t(y, t)$) can be expressed through the following relations (after *Bernoulli-Euler* and *St. Venant* theories):

$$EIw'' = M_b \qquad GK\theta' = M_t \tag{16}$$

where EI and GK accounts for the stiffness response of the structure to bending and torsion.

Consequently, normal (σ_N) and shear (σ_S) stresses distribution have been obtained, employing equations:

$$\sigma_N = \frac{\boldsymbol{M_b}(\boldsymbol{y})}{I} z \qquad \sigma_S = -2\frac{\boldsymbol{M_t}(\boldsymbol{y})}{K} z \tag{17}$$

with I as the area inertia moment, K as torsion constant and z the location of the section where the stress distribution is evaluated.

It is useful to point out that by doing a comparison between $\boldsymbol{v}$ and the same vector obtained applying the *shape functions*, the latter shows slightly higher deformations. Thus, the results from this analysis can be considered to be more conservative (*see functions 'stresses.m' and 'plot_stresses.m' for details on this implementation*).

To say that a structure can *safely* withstand loads to which it is subjected means to verify that the ratio between the *ultimate stress* (values in table 2) and the *limit load*, i.e. the most critical load experienced, is larger than

1.5 (*Safety Factor - SF*).
This check has been done for the three maneuvers analysed in the previous section and are summarized in Table 8 (z location which gives higher stress is the one at the higher distance from the center of the *I-beam* section, i.e. the bottom/top side of the spar cap):

n	σ_N [MPa]	σ_S [MPa]	SF_N	SF_S
1	53.83	33.69	8.97	8.40
4.4	256.54	150.84	1.88	1.88
-1.8	104.95	61.71	4.60	4.59

Table 8: Stresses and *safety factors* for different n ($z = 0.1479$ m).

We see here, that the most critical condition is related to the *pull-up* maneuver. The stresses generated in this case are higher compared to the other two cases, but the structure is still safe.

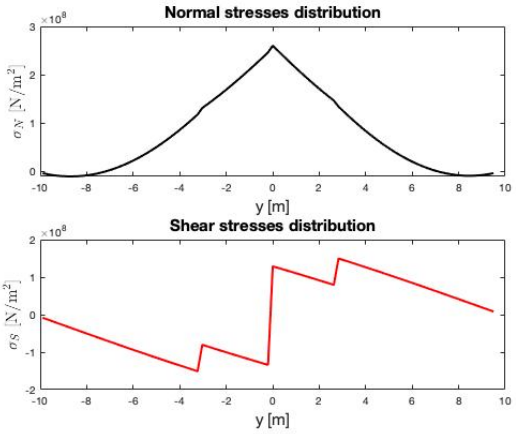

Figure 8: Normal and Shear Stress distributions with *inertial relief*. Plots for $n = 4.4$ and $u = 102$ m/s (lower side of the wing, where tension is experienced).

In figure 8, only the stresses related to this condition are reported.
For the other cases the trend will be the same (opposite with negative load factors).

4.4 Alternative designs

We have shown that, with the sizing described in section 3.2, it is possible to obtain a structure which satisfies all the requirements needed, in such a way to be certified.
Alternative solutions are possible in order to still respect the limitations and improve some aspects (e.g. one of the main objective of a company could be to increase as much as possible the payload). Some of them are described (or introduced) in this section.

Tapered Spar: To increase the payload, by looking at the structure as it is, one solution is to *taper* the dimension of the spar, i.e. to change the parameter $A_c(y)$ along the span.

This has been executed by keeping the dimension of *hspar* constant and varying *bspar*, in such a way that it gets smaller when moving from the root to the tip (this could be easier to achieve when manufacturing, whilst, tapering along the height of the spar cap might be more challenging). Additionally, *tspar* has changed from 5 to 3 mm and t_s is now 0.9 mm.
Table 9 shows the improvements obtained by this design:

$A_c(y)$ [m^2]	t_s [mm]	*Wing Mass* [kg]	*Payload* [kg]
0.01-0.001$\lvert y\rvert$	0.9	667.469	1362.53
0.01	1	992.042	1037.96

Table 9: Mass comparisons with and without tapered spar.

As it can be seen, the tapering, together with the reduction of the wing box thickness, is beneficial, reducing the mass of the wing of more than 30% and increasing the allowable payload of nearly 330 kg. The torsional inertia is reduced to 114.079 kgm^2.

Still, before starting the analysis, the frequency related to the structural response have been checked to assess that they're logical.

f [Hz]	1.125	2.052	3.403	5.937	10.39	16.66

Table 10: Structural frequencies for *tapered* spar.

When carrying out the same tests, as the case for a spar with constant dimensions, we observe that the limiting factor is related to *strength*. Indeed, with this new design, deformations increase.
A big contribution to the stress response is given by the wing box. If further reducing the thickness of the thin sheet we get results that are still acceptable, aeroelastically speaking, but that do not satisfy the safety requirement for the torsional stresses (by reducing t_s of a couple of millimeters more there's also the risk to encounter *buckling*, another effect which may cause damages to the structure).
The *I-beam* spar, instead, helps a lot more when dealing with normal stresses. If increasing the effect of the *taper*, the *safety factor* becomes lower than 1.

The stiffness response is not heavily affected. The structure is still stable from the aeroelastic point of view. Results show a slight reduction of the divergence and the

reversal speed (219.13 m/s and 156.12 m/s) which are still acceptable. *Flutter* is still not encountered up to the divergence speed.

Strut-bracing *(not implemented)*: Design gets more complicated in the case of a *strut-braced wing*, as shown in figure 2.

The idea is to allow for an improved response to the loads acting on the wing, by redistributing part of them over the fuselage. This, theoretically, allows to further reduce the weight of the structure, but, on the other hands, adds a new component of drag, related to an enhancement of flow separation. The two main parameters which have an influence on this drag are the angle of pitch and the lateral angle of inclination of the element. This choice is, actually, a trade-off between the structural response and how much we want to penalize the performances (*see ref. 5*).

Fatigue considerations: Beyond the "pure" structural discussion, also fatigue life has to be taken into consideration. Cyclic loading on the structure, e.g. due to gusts, might lead to crack growth and fatigue failure.

For instance, some care has to be taken when designing the connection between the different parts of the aircraft. A rounded connection is preferred, because it reduces stress concentrations; riveted joints introduce, in contrasts, these stresses, defining critical locations.

The choice is also dictated by the material itself, which, like in the case of the Al 2024-T3, already shows good fatigue-related properties.

5 Conclusion

In this report the main objective has been to show how, for a given design of the main wing of the DHC-6 Twin Otter, tests can be performed to prove that specifications are satisfied and that the wing is *aeroelastically stable* and *structurally safe*.

With the chosen design, it was proved that:

- The divergence and the reversal speed are reasonable and larger than 1.15 v_{ne}.
  On the other hand, it is observed that the wing is *free from flutter*.
- Quasi steady maneuvers, as *pull-up* and *descend*, were studied, including the effect of *inertial relief*. The latter, as expected, shows a beneficial effect, i.e. a reduction of the displacement towards the root.
  Aerodynamic limit was also checked.
- By examining the stresses, it was demonstrated that the structure can *safely* withstand the loads experienced during the whole flight envelope.
- The *tapered spar* design has been implemented. This results into a reduction of more than 30 % of wing mass, when also reducing t_s from 1 to 0.9 mm.
  Stresses are observed to be the limiting factor, whilst the aeroelastic response is affected in a minor sense.
  Other suggestions for improvements are advanced, as *strut-braced* wing and *fatigue-related* considerations.

As every *Finite element* analysis, this one, based on the *strip theory* model, requires further experimental testing.
Still, the importance of this preliminary study, as a solid starting point, was established, together with the reliability of the results.

Bibliography

1. *Aeroelasticity of Slender Wing Structures in Low-Speed Airflow*, D. Borglund, D. Eller, Stockholm, 2016
2. *Roark's Formulas for Stress and Strain*, W. C. Young, R. G. Budynas, A. M. Sadegh, 8th edition, 2012
3. *Determination of Longitudinal Aerodynamic Derivatives Using Flight Data From an Icing Research Aircraft*, R.J. Ranaudo, J.G.Batterson, A.L. Reehorst, T.M. O'Mara, Nevada, 1989
4. *CS-23. Certification Specifications for Normal, Utility, Aerobatic, and Commuter Category Aeroplanes*, European Aviation Safety Agency, 2012
5. *Fluid Dynamic Drag: Practical Information on Aerodynamic Drag and Hydrodynamic Resistance*, S. F. Hoerner, 1965
6. *ASM Aerospace Specification Metals, Inc. : Al 2024-T3 datasheet* (website)
7. *StructX. Tables for hollowed ellipsoid and I-section beam*(website)
8. *SD28010 Aeroelasticity - Course Notes*, 2020
9. *How to Write a Paper*, M. Ashby, Cambridge, 6th edition, 2005